Rezumat

Problema modelarii matematice a relatiei dintre transportul turbulent si parametrii plasmei a fost abordata cu ajutorul unor metode de tip regresie pe o baza de date de dimensiuni medii obtinute cu ajutorul unui cod numeric pentru transport. Acesta din urma imita dinamica particulelor in medii tokamak turbulente cu parametrii relevanti pentru descarcarile de tip AUG. Coeficientii de transport rezultati au fost aproximati cu expresii analitice care sunt capabile sa reproduca dependente individuale cu parametrii plasmei. S-a demonstrat ca un model simplu de regresie globala prezice transportul cu un nivel acceptabil de eroare. Exemple minime de tehnici de învațare automată bazate pe retelele neuronale feed-forward si bayesiene au fost, de asemenea, dezvoltate in vederea etapei viitoare a proiectului.

Au fost studiate moduri de test pe plasma turbulenta luand in considerare proprietatile speciale ale statisticii traiectoriilor ionilor (identificate in prima etapa a proiectului): nivel ridicat de coerenta (reprezentat prim mișcari si corelatii ascunse) si memorie de timp lung a conditiilor initiale. Am gasit o a doua sursa de instabilitate determinata de componentele coerente ale mișcarii, care apare in regimul neliniar al turbulentei. Ea reprezinta un nou mecanism de generare a modurilor de curgere. Am aratat ca ratele de crestere ale modurilor de test sunt functii de timp care determina o comportare oscilatorie a caracteristicilor turbulentei cu frecvente caracteristice foarte mici de ordinul $1/\tau_m$, unde τ_m este timpul de memorie.

Summary

We have tackled the problem of modeling the mathematical relationship between turbulent transport and plasma parameters using regression approaches on a medium-sized database obtained with the aid of a numerical code for transport. The latter mimics the dynamics of particles in turbulent tokamak environments as described by parameters relevant to AUG-like discharges. The resulting transport coefficients were fitted with analytical expressions that are able to reproduce individual dependencies with the plasma parameters. It was shown that a simple global regression model predicts the transport with a fair level of agreement. Minimal examples of machine learning techniques related to feed-forward and Bayesian neural networks have also been developed in view of the future stage of the project.

Test modes on turbulent plasmas were studied taking in to account the special properties of the statistics of ion trajectories (found in the first stage of the project): high level of coherence (represented by hidden motion and correlations) and long memory. We have found a second source of instability determined by the coherent components of the motion, which appears in the nonlinear regime. It represents a new mechanism of generation of zonal flow modes. We have shown that the growth rates of the test modes are functions of time, which determine oscillatory behavior of the characteristics of the background turbulence with very small characteristic frequencies of the order $1/\tau_m$, where τ_m is the memory time.

Effects of hidden coherent motion on the growth rates of turbulence. Modelling of the transport-turbulence dependencies. Programming of Bayesian inference.

Effects of hidden coherent motion on the growth rates of turbulence.

The evolution of turbulence in magnetically confined plasmas is a complex problem that is not completely understood in spite of a huge amount of work (see [1] and the references there in). Low-frequency drift type turbulence, which has a significant influence on plasma confinement, is extensively studied especially in connection with fusion research (see e.g. [2]-[5]).

One of the aims of the project is of fundamental nature and is planned to bring a contribution to a main aspect of strong turbulence, the coherence [1]. More precisely this work (included in the Objective A1) intents to determine and to understand the influence of the quasi-coherent components of the stochastic motion on the evolution of turbulence.

A detailed study of tracer statistics in 2-dimensional incompressible turbulence focused on the analysis of the quasicoherent components of motion was performed in 2022. We have found that the statistical properties are completely different for the trapped (closed, periodic) trajectories compared to the free trajectories that reach large distances. Also, the existence of an average velocity V_d determines strong structural changes by generating coherence in the Lagrangian velocity. We have shown that a slow time variation has not the expected effect of attenuation of the coherent component of the motion, but it determines long-time memory and increases the life of the hidden ordered elements.

The work scheduled for this year (deliverable A2) consists of a theoretical study of the test modes on turbulent plasmas in the case of drift type turbulence. The growth rates and the frequencies of the modes are determined as functions of the characteristics of the background turbulence. The effects of the quasi-coherent components of the ion trajectories are analyzed.

Test modes on turbulent plasmas

Drift waves and instabilities are low-frequency modes generated in non-uniform magnetically confined plasmas. Since the aim of this work is to understand the effects of trapping on the evolution of turbulence, we consider a simple confining geometry, the plane plasma slab, in which the magnetic field is straight and uniform. Plasma has low β, which means that the perturbation of the magnetic field is negligible (electrostatic approximation).

The magnetic field is along z axis ($\mathbf{B} = B\mathbf{e}_z$) and plasma is non-uniform in the radial direction taken along x axis. For simplicity, the equilibrium temperatures are uniform and only the density $n_0(x)$ is x-dependent. The characteristic length of density variation $L_n = n_0/|dn_0/dx|$ is much larger than the wave length of the drift modes.

We start from the basic description of this (universal) drift turbulence provided by the drift kinetic equation in the collisionless limit. Drift modes are represented by wave type potential $\delta\phi(x,y,z,t) = \phi_{k\omega}\exp\left(ik_x x + ik_y y + ik_z z - i\omega t\right)$, where k_i are the components of the wave number and ω is the frequency (with imaginary part γ). They have

$$k_z \ll k_x, k_y, v_{Ti} \ll \omega/|k_z| \ll v_{Te}$$

where v_{Te}, v_{Ti} are the thermal velocities of electrons and ions. The solution of the dispersion relation, which is the quasineutrality condition, is (see [27])

$$\omega = \frac{k_y V_{*e}}{1 + k_\perp^2 \rho_s^2}$$
$$\gamma = \sqrt{\frac{\pi}{2}} \frac{\omega\left(k_y V_{*e} - \omega\right)}{|k_z| v_{Te}}$$

where $\mathbf{V}_{*e} = V_{*e}\mathbf{e}_y, V_{*e} = T_e/(eBL_n) = \rho_s c_s/L_n$ is the diamagnetic velocity, $\rho_s = c_s/\Omega_i, c_s = \sqrt{T_e/mi}, T_e$ is the electron temperature, m_i is the ion mass, e is the absolute value of electron charge, $\Omega_i = eB/m_i$ is the cyclotron frequency of the ions and $k_\perp = \sqrt{k_x^2 + k_y^2}$ is the perpendicular wave number. Drift modes are unstable ($\gamma > 0$) if $\omega < k_y V_{*e}$. The ρ_s dependence that appears in (2) yields from the ion polarization drift

$$\mathbf{u}_p = -\frac{m_i}{eB^2}\partial_t \mathbf{E}_\perp$$

The solution in the limit $\rho_s = 0$ (obtained by neglecting the polarization drift) is $\omega = k_y V_{*e}, \gamma = 0$, which represents the stable drift waves. For an arbitrary initial condition ϕ_0, this solution is

$$\phi(x,y,z,t) = \phi_0(x, y - V_{*e}t, z).$$

It shows that any potential ϕ_0 in a non-uniform plasma moves with the diamagnetic velocity. Finite Larmor radius effects, collisions or other perturbations determine supplementary time dependences that modify the potential amplitude and shape but this usually appears on larger time scale.

Drift type instabilities appear for a large range of wave numbers and produce a turbulent potential.

Test mode models consider a turbulent plasma with given statistical characteristics of the background potential $\phi_b(\mathbf{x}, z, t)$ and a small perturbation $\delta\phi, \phi = \phi_b + \delta\phi$. The growth rates and the frequencies of the test modes are determined as functions of the statistical characteristics of ϕ_b. The potential ϕ_b is taken as the zero ρ_s solution (5). The modification of potential shape and amplitude appears due to polarization drift on a larger time scale of the order $1/\gamma$. The test mode studies of turbulence are based on this time scale separation, which permits a sequential approach. Starting from a potential that is a zero order solution (5) it is possible to determine the frequency and the growth rate of test modes as function of the statistical characteristics of the potential. They provide information on the tendency in the

evolution of the potential, which is used to determine the test mode properties later in the evolution, and so on. We have developed such iterated approach for the drift turbulence [10], [11] (the iterated self-consistent method - ISC) based on semianalytical estimations of the Lagrangian statistics. The present results are based on the detailed numerical study of ion trajectories performed in 2022, which identifies important new aspects and reveals the complexity of the Lagrangian statistics.

The main statistical characteristics of the background turbulence are the amplitude Φ of the potential fluctuations, their correlation lengths λ_x, λ_y and correlation time τ_c. They appear in the Eulerian correlation (EC) of the potential (the Fourier transform of the spectrum) defined by

$$E(\mathbf{x}, t) \equiv \langle \phi_b(\mathbf{x}', t')\phi_b(\mathbf{x}' + \mathbf{x}, t' + t)\rangle$$

where $\langle\rangle$ is the statistical average or the space average. This function is the Fourier transform of the spectrum. The amplitude of the stochastic electric drift is $V = \sqrt{V_x^2 + V_y^2}$, where $V_x = \Phi/B\lambda_y, V_y = \Phi/B\lambda_x$. These parameters define the time of flight (or the eddying time) $\tau_{fl} = \lambda_x/V_x = \lambda_x\lambda_y B/\beta$, which is the characteristic time for trajectory trapping.

The perturbations of the electron and ion distribution functions as response to the potential $\delta\phi$ have to be determined as functions of the EC of the background turbulence.

The electrons have the same response to a perturbation $\delta\phi$ as in quiescent plasma due to their fast parallel motion

$$\delta n^e = n_0(x)\frac{e\delta\phi}{T_e}\left(1 + i\sqrt{\frac{\pi}{2}}\frac{\omega - k_y V_{*e}}{|k_z|v_{Te}}\right)$$

[see, for example, [27], page 457].

The distribution of the ions $f^i(\mathbf{x}, \mathbf{v}, t)$ in a stochastic potential $\phi_b(\mathbf{x}, t)$ is solution of the drift kinetic equation

$$O^i f^i + f^i \nabla \cdot \mathbf{u}_p = 0$$
$$O^i \equiv \partial_t - \frac{\nabla\phi_b \times \mathbf{b}}{B} \cdot \nabla$$

where O^i is the derivative along ion trajectories. The parallel motion is negligible due to condition (1). The distribution

$$f_0^i = n_0(x)F_M^i \exp\left(\frac{e\phi_b(\mathbf{x} - \mathbf{V}_{*e}t)}{T_e}\right)$$

represents the short time approximate equilibrium because $O^i f_0^i = 0$ and the term $\nabla \cdot \mathbf{u}_p \ll 1$ can be neglected. Perturbing the potential with

$$\delta\phi(x,y,t) = \phi_{k\omega}\exp\left(ik_x x + ik_y y + ik_z z - i\omega t\right)$$

the operator is perturbed with

$$\delta O^i = -\frac{1}{B}\nabla\delta\phi \times \mathbf{e}_z \cdot \nabla = \delta\mathbf{v}\cdot\nabla$$

and a change of the distribution function appears $f^i = f_0^i + h$. The linearized equation in this perturbation is

$$O^i h + h\nabla\cdot\mathbf{u}_p = -\delta O^i f_0^i - f_0^i \nabla\cdot\delta\mathbf{u}_p$$

with the rhs terms

$$\begin{gathered}\delta O^i f_0^i = ik_y V_{*e} n_0(x) F_M^i \frac{e\delta\phi}{T_e}\exp\left(\frac{e\phi_b(\mathbf{x}-\mathbf{V}_{*e}t)}{T_e}\right) - i\left[k_x v_x + k_y v_v\right] n_0(x) F_M^i \frac{e\delta\phi}{T_e}\exp\left(\frac{e\phi_b(\mathbf{x}-\mathbf{V}_{*e}t)}{T_e}\right) \\ f_0^i\nabla\cdot\delta\mathbf{u}_p = -f_0^i\,\partial_t\Delta\delta\phi = n_0(x)F_M^i\exp\left(\frac{e\phi_b(\mathbf{x}-\mathbf{V}_{*e}t)}{T_e}\right)(i\omega\rho_s^2 k_\perp^2)\frac{e\delta\phi}{T_e}\end{gathered} \tag{1}$$

The second term in $\delta O^i f_0^i$ (the advection of the background potential with the perturbation of the velocity) is usually neglected. We show here that it yields a significant contribution due to the coherent elements of the ion trajectories

The equation for the response h is

$$\begin{aligned}O^i h + h\nabla\cdot\mathbf{u}_p = -in_0(x)F_M^i\frac{e\phi_{k\omega}}{T_e}\left(k_y V_{*e} + \left(k_x v_x + k_y v_v\right) - \omega\rho_s^2 k_\perp^2\right) \\ \exp\left(ik_x x + ik_y y + ik_z z - i\omega t + \frac{e\phi_b(\mathbf{x}-\mathbf{V}_{*e}t)}{T_e}\right)\end{aligned}$$

The formal solution is obtained by the method of the characteristics as

$$h(\mathbf{x},v,t) = -n_0(x)F_M^i\frac{e\phi_{k\omega}}{T_e}\left(k_y V_{*e} - \omega\rho_s^2 k_\perp^2\right)\bar{\Pi}_1^i - n_0(x)F_M^i\frac{e\phi_{k\omega}}{T_e}\bar{\Pi}_2^i \tag{2}$$

where the propagators are

$$\bar{\Pi}_1^i = i\int_{-\infty}^t d\tau\langle M(\tau,t)\rangle\exp\left[-i\omega(\tau-t)\right] \tag{3}$$

$$\bar{\Pi}_2^i = i\int_{-\infty}^t d\tau\left\langle\left(k_i v_{ib}(\mathbf{x}(\tau)-\mathbf{V}_{*e}\tau)\right)M(\tau,t)\right\rangle\exp\left[-i\omega(\tau-t)\right] \tag{4}$$

and $M(\tau)$ is

$$M(\tau,t) \equiv \exp\left[\frac{e\phi_b(\mathbf{x}-\mathbf{V}_{*e}t)}{T_e} + i\mathbf{k}\cdot(\mathbf{x}(\tau)-\mathbf{x}) - \int_\tau^t d\tau'\nabla\cdot\mathbf{u}_p\left(\mathbf{x}(\tau')\right)\right] \tag{5}$$

The integrals are along ion trajectories obtained from Eq. (20) calculated backwards in time with the condition at $\tau = t, \mathbf{x}(t) = \mathbf{x}$.

The average of the function $M(\tau, t)$ is determined in two steps: first on the subensemble of the trajectories that start from fixed values of the potential $\phi_b(\mathbf{x}, t) = \phi^0$ (averages conditioned by ϕ^0) and and secon on the whole statistical ensemble by averaging over ϕ^0.

$$\begin{aligned} M^{\phi^0}(\tau, t) &= \langle M(\tau, t)\rangle_{\phi^0} \\ \langle M(\tau, t)\rangle &= \int_{-\infty}^{\infty} d\phi^0 \langle M(\tau, t)\rangle_{\phi^0} P(\phi^0) \end{aligned} \tag{6}$$

where $P(\phi^0) = 1/\sqrt{2\pi}\exp\left(-(\phi^0/\Phi)^2/2\right)$. This procedure enables the analysis of the effects of the coherent components of the motion found in trajectory statistics.

$$\begin{aligned} M^{\phi^0}(\tau, t) = &\exp\left[\frac{e\langle\phi_b(\tau)\rangle_{\phi^0}}{T_e} + i\mathbf{k}\cdot\langle(\mathbf{x}(\tau) - \mathbf{x})\rangle_{\phi^0} - \int_\tau^t d\tau' \left\langle \nabla\cdot\mathbf{u}_p\big(\mathbf{x}(\tau')\big)\right\rangle_{\phi^0}\right] \\ &\exp\left[\frac{e^2\langle(\delta\phi_b(\tau))^2\rangle_{\phi^0}}{2T_e^2} - \frac{k_i k_j\left\langle\big(\delta(x_i(\tau) - x_i)\big)\big(\delta(x_j(\tau) - x_j)\big)\right\rangle_{\phi^0}}{2}\right] \\ &\exp\left[ik_i\frac{e\left\langle(\delta\phi_b(\tau))\big(\delta(x_i(\tau) - x_i)\big)\right\rangle_{\phi^0}}{T_e} - \frac{e}{T_e}\int_\tau^t d\tau' \left\langle \delta\phi_b(\tau)\nabla\cdot\mathbf{u}_p\big(\mathbf{x}(\tau')\big)\right\rangle_{\phi^0}\right] \\ &\exp\left[-ik_i\int_\tau^t d\tau' \left\langle\big(\delta(x_i(\tau) - x_i)\big)\nabla\cdot\mathbf{u}_p\big(\mathbf{x}(\tau')\big)\right\rangle_{\phi^0}\right] \end{aligned} \tag{7}$$

where $\phi_b(\mathbf{x}(\tau) - \mathbf{V}_{*e}\tau) \equiv \phi_b(\tau)$ and $i, j = x, y$. The compressibility term depends on the vorticity $\zeta(\mathbf{x}, t) = \Delta\phi_b(\mathbf{x}, t)$

$$\int_\tau^t d\tau' \nabla\cdot\mathbf{u}_p\big(\mathbf{x}(\tau')\big) = -\frac{m_i}{eB^2}\int_\tau^t d\tau'\, \partial_{\tau'}\zeta(\tau')$$

Most of the term in the above exponential function represent coherent components of ion trajectories or are influenced by them, as discussed below.

Stochastic and coherent aspects of the trajectories

We analyze the Lagrangian averages that appear in Eq. (7) and present a short review of the results reported in 2022 adapted to the present study.

The equation of the trajectories / characteristics in the system that moves with the potential (with the diamagnetic velocity V_*) is

$$\frac{d\mathbf{x}}{dt'} = -\nabla\phi\times\mathbf{e}_3 + V_d\mathbf{e}_2 \equiv \mathbf{v}_t(\mathbf{x}, t') \tag{8}$$

where $\mathbf{e}_1, \mathbf{e}_2$ are the unit vectors in the plane perpendicular to the confining magnetic field $\mathbf{B} = B\mathbf{e}_3$, and $\mathbf{x} = (x_1, x_2)$. The equation is written is a system that moves with the background potential using dimensionless quantities with the potential normalized by its amplitude $\Phi(\phi = \phi_b/\Phi)$, the distances by ρ_s, the velocities by $V_e = \Phi/(B\rho_s)$ (a measure of the electric drift) and the time by $\tau_{fl} = \rho_s/V_e = B\rho_s^2/\Phi$ (a measure of the time of flight). The average velocity V_d is the normalised diamagnetic velocity $V_d = V_{*e}/V_e$.

These units for time and velocity were chosen because they evidence the combined effects of plasma rotation and of the turbulence amplitude. The elements of the statistics of trajectories that appear in Eq. (19) are expressed in physical units, which are obtained by scaling the time with τ_{fl} and by multiplying the velocities with V_e. They are also useful because they provide in a simple way the main dependences on the amplitude of background potential Φ. The increase of Φ determines the decrease of V_d and the "contraction" of time

$$V_d = \frac{V_{e*}}{V_e} = \left(\frac{e\Phi}{T_e}\frac{L_n}{\rho_s}\right)^{-1},\ \tau_{fl} = \frac{\rho_s^2 B}{\Phi}$$

We have examined the statistical properties of subensembles of trajectories that start from fixed values of the potential, ϕ^0 (conditioned statistics). At any value of ϕ^0, there are two categories of trajectories: trapped (closed, periodical, with small displacements) and free (non-periodical with large displacements). The have found completely different statistics for these categories in the static potential where they can be defined. The initial potential on the free trajectories is Gaussian

$$P^{fr}(\phi^0) = \frac{1}{\sqrt{2\pi}\Delta}\exp\left(-\frac{(\phi^0)^2}{2\Delta^2}\right)$$

where the width $\Delta < \Phi$ is a decreasing function of Φ that evolve from 1 at small Φ $\left(\frac{e\Phi}{T_e} \ll \frac{\rho_s}{L_n}\right)$ to 0 at very large Φ $\left(\frac{e\Phi}{T_e} \gg \frac{\rho_s}{L_n}\right)$, approximated by

$$\Delta = \left[1 - \exp\left(-\left(\frac{T_e}{e\Phi}\frac{\rho_s}{L_n}\right)^2\right)\right]^{0.17}$$

This shows that at small Φ all the trajectories are free, and Φ progressively closes the trajectories as the amplitude of the background potential increases. This precess begins when $\frac{e\Phi}{T_e} \gtrsim \frac{\rho_s}{L_n}$ and determines the tranzition from the completely random trajectories to the nonlinear Lagrangian statistics that is caracterised by complex effects (as trajectory trapping, generation of coherence and of memory effects). The trapped trajectories start from values of the initial potential ϕ^0 that have the complementary distribution

$$P^{tr}(\phi^0) = P(\phi^0) - P^{fr}(\phi^0)$$

The fractions of free $n^{fr}(\phi^0)$ and trapped $n^{tr}(\phi^0)$ trajectories that evolve on ϕ^0 contour lines are related to these probabilitie

$$n^{fr}(\phi^0) = n_{fr}P^{fr}(\phi^0),\ n^{tr}(\phi^0) = n_{tr}P^{tr}(\phi^0),$$

where n_{fr} and n_{tr} are the total fractions of each category. They are compared in Fig. 1 to the distribution of the Lagrangian potential $P(\phi^0)$ and to the above analytical approximations (solid lines), respectively. n_{fr} depends on Φ with monotonic decay from 1 to 0

$$n_{fr} = \left[1 - \exp\left(-\left(\frac{T_e}{e\Phi}\frac{\rho_s}{L_n}\right)^2\right)\right]^{1/4}$$

The main result of this study is the identification of coherent motions, which appear for the free trajectories in each subensemble of trajectories that evolve on ϕ^0 contour lineas. They are represented by average displacements conditioned by $\phi^0, \langle x_i(t)\rangle_{\phi^0,fr}$.

The perpendicular average displacement $\langle x_1(t)\rangle_{\phi^0}P(\phi^0)$ has the sign of ϕ^0, as seen Fig. 1 (blue points). This coherent displacement has a fast time increase followed by saturation, as seen in Fig. 2 (black dashed line). Collecting the positive and the negative displacements, a pair of transitory average velocities perpendicular on $\mathbf{V}_d$ conditioned by the sign of ϕ^0 is found. These are the hidden drifts, which have opposite directions and exactly compensate each other.

The other elements of the statistics of the free trajectories conditioned by ϕ^0 (like $\langle x_2(t)\rangle_{\phi^0,fr}, \left\langle \delta x_i^2(t)\right\rangle_{\phi^0,fr}\Big)$ do not dependent on ϕ^0, which means that the free trajectories with different values of ϕ^0 are statistically identical, except for the perpendicular average displacement that is $\langle x_1(t)\rangle_{\phi^0,fr} = \phi^0/V_d$.

We have also found that the Lagrangian potential $\phi(\mathbf{x}(t))$ and vorticity $\omega(\mathbf{x}(t))$ show conditional order represented by averages proportional to ϕ^0. They are essentially produced by the trapped trajectories, because $\langle\phi(\mathbf{x}(t))\rangle_{\phi^0,tr}$, $\langle\omega(\mathbf{x}(t))\rangle_{\phi^0,tr}$ are time invariant, while the contributions of the free trajectories decay to zero. This is a selective decorrelation mechanism, that is induced by V_d through the structure of the contour lines of the potentials and affects only the free trajectories. The typical time evolution of $\langle\phi(\mathbf{x}(t))\rangle_{\phi^0}$ and $\langle\omega(\mathbf{x}(t))\rangle_{\phi^0}$ is shown in Fig. 2 by the blue and red dashed lines. The asymptotic values $\langle\phi(\mathbf{x}(t))\rangle_{\phi^0}P(\phi^0) \to \phi^0 n^{tr}(\phi^0), \langle\omega(\mathbf{x}(t))\rangle_{\phi^0}P(\phi^0) \to -\phi^0(1/\lambda_1^2 + 1/\lambda_2^2)n^{tr}(\phi^0)$ are attained in a short time.

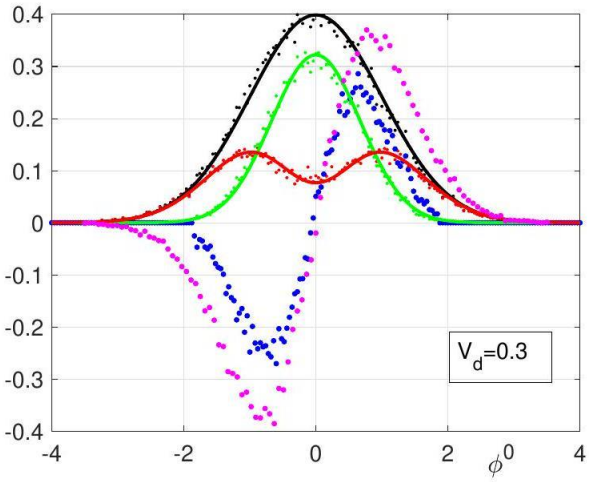

FIG. 1: Main elements of the Lagrangian statistics conditioned by ϕ^0. The fractions of trajectories at saturation: $P(\phi^0)$ (black) and its components $n^{fr}(\phi^0)$ (green) and $n^{tr}(\phi^0)$ (red). The conditioned perpendicular average $\langle x_1\rangle_{\phi^0} P(\phi^0) * V_d$ for $\tau_c = \infty$ (blue poins) and $\tau_c = 33$ (magenta points).

Equation (17) shows that the Lagrangian averages conditioned by ϕ^0 are always functions of ϕ^0 (even when the average is determined only by one category and does not depend on ϕ^0). As a result, the correlations of the fluctuations

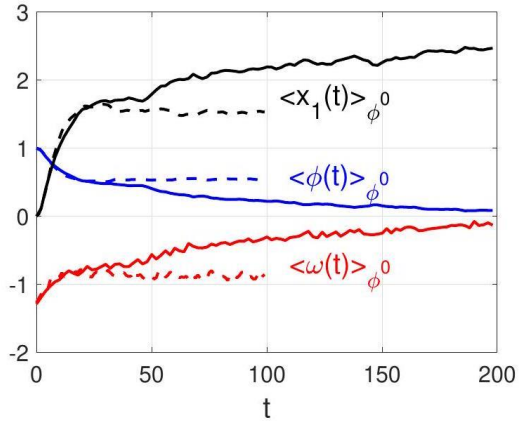

FIG. 2: Effects of the time dependence of the potential: time evolution of the averages conditioned by the initial potential for the perpendicular displacements, the Lagrangian potential and the vorticity in frozen (dashed lines) and time dependent (solid lines) potentials. $\phi^0 = 1, V_d = 0.3$ and $\tau_c = 33$.

(as $\langle \delta x_i^2(t)\rangle_{\phi^0}$) contain the averages (the ordered motion), because $\langle x_i(t)\rangle_{\phi^0}$ and $\langle x_i(t)\rangle_{\phi^0,c}$ do not compensate in the equations of the type writted for $x_i^2(t)$. Thus, the hidden coherence influences the correlations of the Lagrangian fluctuations (including the transport). This process is explicitly presented in the next sections for the stochastic advection of fields.

The statistics of the free and trapped trajectories obtained by adding the contribution of all contour lines (by integrating over ϕ^0) has completely different properties for the two categories. The probability

of displacements $P_{tr}(x_1, x_2, t)$ of the trapped trajectories is a narrow peak around $\mathbf{x} = \mathbf{0}$. The distribution of the free trajectories $P_{fr}(x_1, x_2, t)$ is a Gaussian with much larger extension (especially in the parallel direction where it increases in time), which moves along $\mathbf{V}_d$ with the velocity $V_d/n_{fr} > V_d$. These two contributions appear separately in the total probability $P(x_1, x_2, t)$, as seen in Fig. 3 (blue lines). The asymptotic transport is dominated by the coherent motion. a

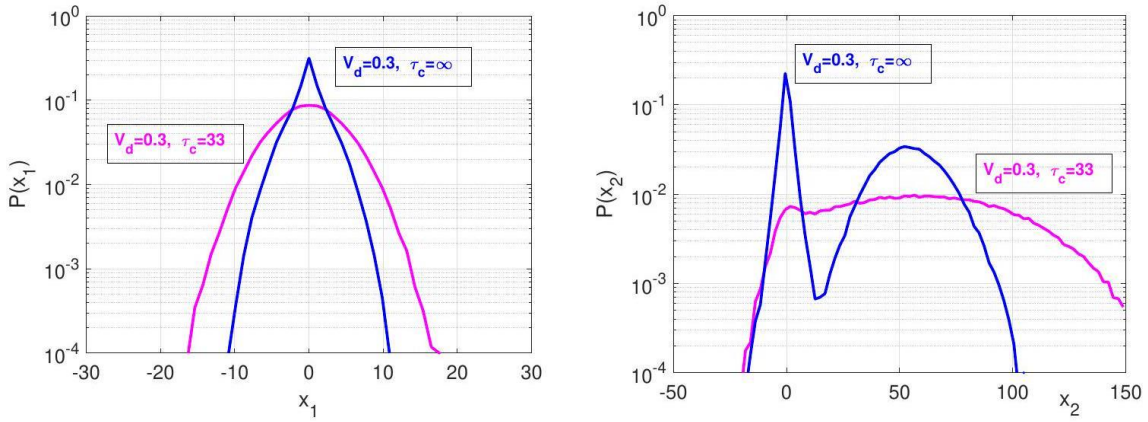

FIG. 3: The probability of displacements across (left panel) and along (right panel) the average velocity $\mathbf{V}_d$ for frozen potential (blue) and for time-dependent potential with $\tau_c = 33$ (magenta).

In the case of time dependent potentials the trajectories cannot be organized according to the categories, because closed trajectories cannot exist. However, at slow time variation of the potential, random trapping events exist (as intervals of eddying motion) on all trajectories calculated for long time. This are separated by long jumps that are similar with the free trajectories. The statistical analysis can be conditioned only by the initial potential ϕ^0.

The results obtained in time-dependent potentials are rather surprising. Instead of the expected decay after the decorrelation time, a strong increase of the Lagrangian coherence is found. The average conditioned by ϕ^0 of the perpendicular displacements $x_1(t)$ significantly increase, as seen in Fig. 2 (black solid line). The time derivative of $\langle x_1(t)\rangle_{\phi^0}$ does not vanish as in frozen potential, but it exists even for $t \gg \tau_c$. This determines a long life of the hidden drifts.

The stochastic time variation determines total decorrelation of the conditioned Lagrangian potential $\langle\phi(\mathbf{x}(t))\rangle_{\phi^0}$, but this is a very slow process. As seen in Fig. 2 (blue solid line), $\langle\phi(\mathbf{x}(t))\rangle_{\phi^0}$ still has a significant value at $t = 200 \cong 6\tau_c$ where the Eulerian correlation is $E(\mathbf{0}, 200) = 10^{-8}$. The Lagrangian vorticity $\omega(\mathbf{x}(t))$ has similar behavior, except the sign, which is opposite to the sign of $\langle\phi(\mathbf{x}(t))\rangle_{\phi^0}$. Both quantities have very long memory of the initial condition.

The time evolution of the average velocity, Lagragian potential and vorticity are all governed by the same law, as seen in Fig. 4. This defines the memory function and the memory time τ_m

$$F_m = \exp\left(-\frac{t}{\tau_m}\right) \qquad (9)$$

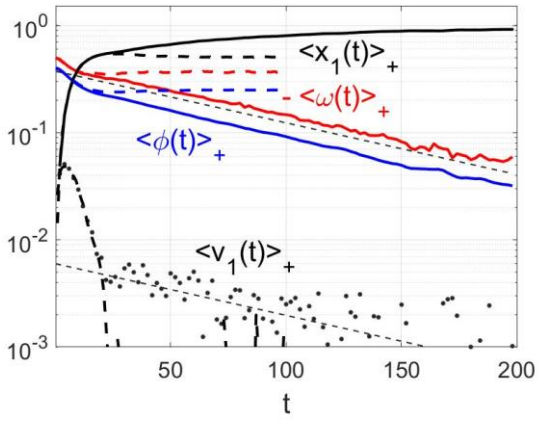

FIG. 4: The time dependence of the average radial displacement, velocity, Lagragian potential and vorticity, conditioned by the sign of the initial potential ϕ^0 for the frozen (dashed) and the time-dependent (solid) cases. The thin dashed lines are $\sim \exp\left(-\frac{t}{90}\right)$, $V_d = 0.3$ and $\tau_c = 33$.

The probability of displacements $P(x_1, x_2, t)$ is strongly modified in time-dependent potentials, as seen in Fig. 3 (magenta lines). A trace of the contribution of the trapped trajectories can still be observed, but the shape of P is completely different. It contributes to the conclusion that the trajectories conditioned by the initial potential become statistically identical for all values of ϕ^0, not only on the domain of small potential with width Δ, as in frozen potentials.

The long memory and the enhanced coherence are effects of the stochastic liberation of the trajectories that initially are trapped, followed by repeated stochastic captures that are constraint by the approximate invariance of the total potential.

- *The averages in the propagators*

The characteristics and approximations of the main averages that appear in Eq. (7) are discussed below and shown in Figs. 5-9.

The radial displacements have dominant coherent behavior represented by an average that appears only for the free trajectories in static potentials and has the sign of ϕ^0

$$\langle x_1(t) - x_1(0)\rangle_{\phi^0} P(\phi^0) = \frac{\phi^0}{V_d B} n^{fr}(\phi^0)$$

In time dependent potentials this coherent motion increases and extends to the whole domain of ϕ^0, as seen in Fig 1 fig1_fidp by coparing the magenta and blue points. We approximate this quantity by retaining the main feature, which is the coincidence of its sign with the sign of ϕ^0. The dependence on ϕ^0 is eliminated by integrating on the positive and negative domains

$$\langle x_1(t) - x_1(0)\rangle_+ = \int_0^\infty \langle x_1(t) - x_1(0)\rangle_{\phi^0} P(\phi^0) d\phi^0, \quad \langle x_1(t) - x_1(0)\rangle_- = -\langle x_1(t) - x_1(0)\rangle_+$$

These coherent displacements and the corresponding average velocities can be approximated by (in physical units)

$$\langle x_1(t) - x_1(0)\rangle_{sg} = \rho_s sg \left[g_1^{x_1} \left(1 - \exp\left(-\frac{t}{\tau_m} \right) \right) + g_2^{x_1} \right]$$

$$\langle v_1(t)\rangle_{sg} = V_e sg \frac{g_1^{x_1}}{\tau_m} \exp\left(-\frac{t}{\tau_m} \right)$$

$\langle x_1(t) - x_1(0)\rangle_{\text{sg}}$ is approximately linear in time for intervals of the order $50\tau_{fl} >> \tau_*$, which enable the use of

$$\langle x_1(\tau) - x_1(t)\rangle_{sg} \cong \tau_{fl} \langle v_1(\tau)\rangle_{sg} (t - \tau)$$

in the propagators (in the time integrals).

The amplitudes of the fluctuations $\left\langle \left(\delta(x_i(\tau) - x_i)\right) \left(\delta\left(x_j(\tau) - x_j\right)\right) \right\rangle_{\phi^0}$ are subdiffusive in the radial direction and superdiffusive in the poloidal direction

$$\left\langle \left(\delta(x_1(t) - x_1)\right)^2 \right\rangle_{\phi^0} \cong \rho_s^2 \left(\frac{t}{\tau_{fl}} \right)^{\alpha_1},$$

$$\left\langle \left(\delta(x_2(t) - x_2)\right)^2 \right\rangle_{\phi^0} \cong \rho_s^2 \left(\frac{t}{\tau_{fl}} \right)^{\alpha_2},$$

where $\alpha_1 < 1$ and $\alpha_2 > 1$. They have a weak dependence on ϕ^0, which can be ignored. The diffusion coefficients are

$$D_{11}(t) = \rho_s V_e \alpha_1 \left(\frac{t}{\tau_{fl}} \right)^{\alpha_1 - 1}, \; D_{22}(t) = \rho_s V_e \alpha_2 \left(\frac{t}{\tau_{fl}} \right)^{\alpha_2 - 1}$$

The linear approximation on intervals used for $\langle x_1(\tau) - x_1(t)\rangle_{sg}$ can be applied in this case because the time variation is slow

$$\left\langle \left(\delta(x_i(\tau) - x_i(t))\right)^2 \right\rangle \cong \tau_{fl} D_{ii}(\tau)(t - \tau)$$

There is cross correlation of the displacements that is roughly linear in ϕ^0, as seen in Fig. croscorel

$$\left\langle \left(\delta(x_i(\tau) - x_i)\right) \left(\delta\left(x_j(\tau) - x_j\right)\right) \right\rangle_{\phi^0} \cong \rho_s^2 g^{12} \frac{\phi^0}{\Phi}$$

The Lagrangian potential has in the presence of trapping a coherent component with long time memory

$$\langle \phi_b(\tau)\rangle_{\phi^0} = \Phi\phi^0 \exp\left(-\tau/\tau_m\right)$$

that is linear in ϕ^0. The conditioned fluctuations $\langle(\delta\phi_b(\tau))^2\rangle_{\phi^0}$ have time-increasing amplitude (from zero to the Eulerian value Φ) with negligible dependence on ϕ^0. The Lagrangian vorticity has very similar properties with the potential. Its coherent component has the same dependence on ϕ^0 and time

$$\langle \zeta(\tau)\rangle_{\phi^0} = \frac{\Phi}{\rho_s^2} g^{\zeta}\phi^0 \exp\left(-\tau/\tau_m\right)$$

where g^{ζ} depends on the spectrum of the turbulence (on the correlation lenghts). Since $\tau_m >> \tau_*$, the liniar approximations can be used in the propagators

$$\langle \phi_b(\tau)\rangle_{\phi^0} \cong \langle \phi_b(t)\rangle_{\phi^0}\left(1-\frac{\tau-t}{\tau_m}\right),\ \langle \zeta(\tau)\rangle_{\phi^0} \cong \langle \zeta(t)\rangle_{\phi^0}\left(1-\frac{\tau-t}{\tau_m}\right).$$

The average of the compressibility term is

$$\int_{\tau}^{t} d\tau' \left\langle \nabla\cdot\mathbf{u}_p\left(\mathbf{x}(\tau')\right)\right\rangle_{\phi^0} = -\frac{m_i}{eB^2}\int_{\tau}^{t} d\tau'\,\partial_{\tau'}\langle\zeta(\tau')\rangle_{\phi^0} \cong -\frac{V_e}{c_s}\frac{\tau-t}{\tau_m}.$$

The correlation of the radial displacements $\delta(x_1(\tau)-x_1)$ with the vorticity $\zeta(\tau')$ is a slowly increasing function of time that depends weakly on ϕ^0 and can approximated by

$$\langle \delta(x_1(\tau)-x_2)\zeta(\tau')\rangle_{\phi^0} \cong \frac{\Phi}{\rho_s} g^{\zeta 1}\exp\left(\frac{\tau-\tau'}{\tau_m}\right)$$

with $g^{\zeta 1} \cong 0.3$, while the poloidal displacements yield a roughly constant time function with linear dependence in ϕ^0

$$\langle \delta(x_2(\tau)-x_2)\zeta(\tau')\rangle_{\phi^0} \cong \frac{\Phi}{\rho_s} g^{\zeta 2}\frac{\phi^0}{\Phi}$$

where $g^{\zeta 2} \cong 13$. The correlations with the compressibility terms are

$$\begin{aligned}\int_{\tau}^{t} d\tau' \left\langle \delta(x_1(\tau)-x_1)\nabla\cdot\mathbf{u}_p\left(\mathbf{x}(\tau')\right)\right\rangle_{\phi^0} &= -\frac{m_i}{eB^2}\frac{\Phi}{\rho_s} g^{\zeta 1}\left(\exp\left(\frac{t-\tau}{\tau_m}\right)-1\right)\\ &= -\rho_s\frac{V_e}{c_s} g^{\zeta 1}\frac{\tau-t}{\tau_m}\\ \int_{\tau}^{t} d\tau' \left\langle \delta(x_2(\tau)-x_2)\nabla\cdot\mathbf{u}_p\left(\mathbf{x}(\tau')\right)\right\rangle_{\phi^0} &= -\rho_s\frac{V_e}{c_s} g^{\zeta 2}\frac{\phi^0}{\Phi}\end{aligned}$$

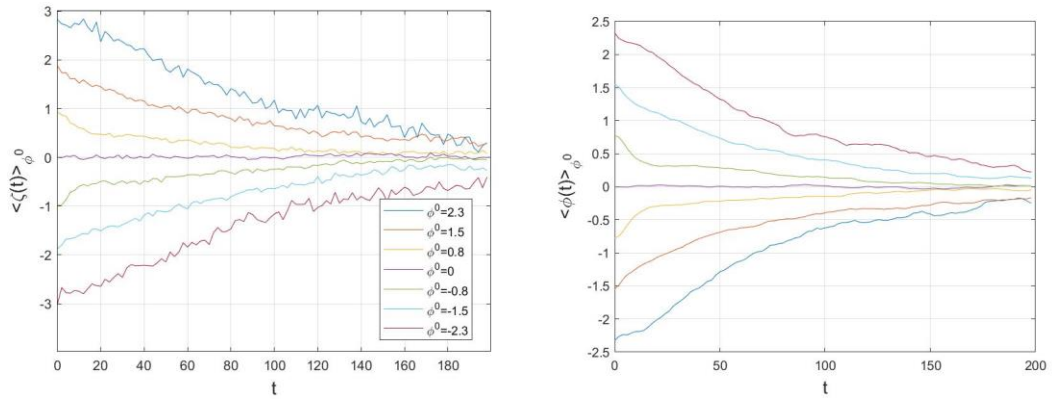

FIG. 5: The time dependence of the average Lagrangian vorticity (left) and potential (right) conditioned by the initial potential ϕ^0 for several values of ϕ^0. Memory effects are seen and the linear dependence on ϕ^0. $V_d = 0.3$ and $\tau_c = 33$.

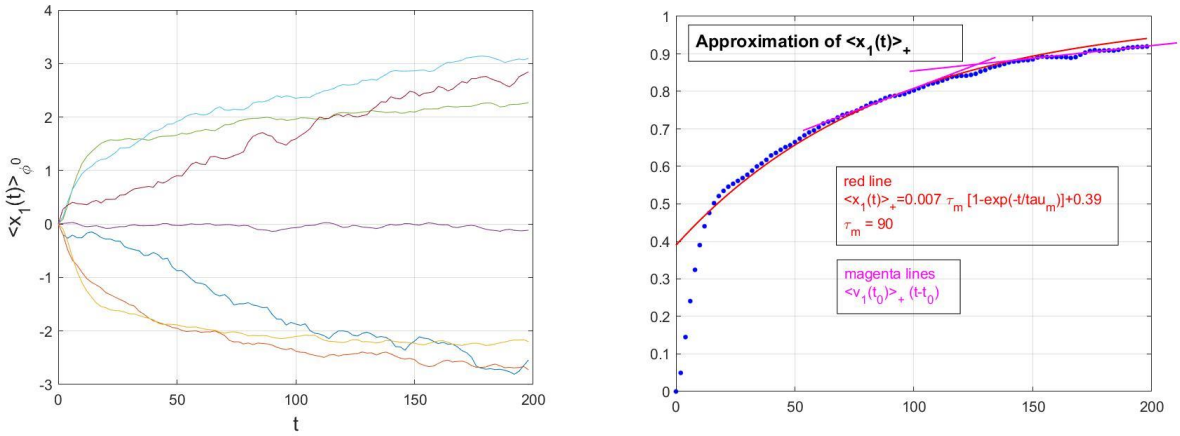

FIG. 6: The time dependence of the average radial displacement conditioned by ϕ^0 (left) and by the positive sign of ϕ^0 (right). Also shown in the left panel are the approximations over memory time (red) and linear approximations (magenta). $V_d = 0.3$ and $\tau_c = 33$.

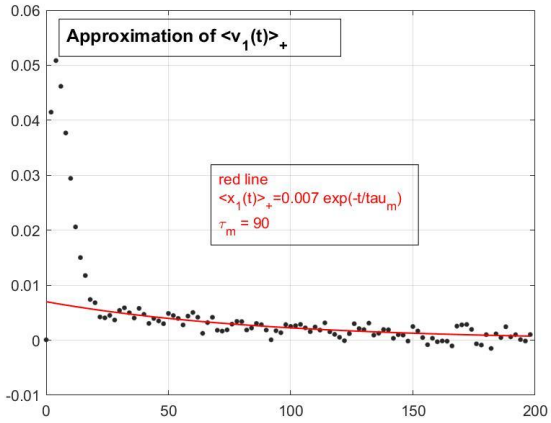

FIG. 7: The time dependence of the average radial velocity conditioned by the positive sign of ϕ^0 (points) and its approximation (red). $V_d = 0.3$ and $\tau_c = 33$.

Correlations between the trajectories and the Lagrangian potential appear in both directions. In the radial direction, the correlation does not depend on ϕ^0, is negative and its absolute value increases in time and saturates

$$\left\langle (\delta\phi_b(\tau))\big(\delta(x_1(\tau) - x_1)\big)\right\rangle_{\phi^0} \cong -\Phi\rho_s g^{\phi 1},\ \tau - t \gtrsim \tau_c$$

where $g^{\phi 1} \cong 2$. In the poloidal direction, the correlations are stronger, reaching values up to 10 . They are increasing functions of time as well, which saturate at values that depend linearly on ϕ^0

$$\left\langle (\delta\phi_b(\tau))\big(\delta(x_2(\tau) - x_2)\big)\right\rangle_{\phi^0} \to -\phi^0\Phi\rho_s g^{\phi 2}$$

where the $g^{\phi 2} \cong 5$. The product of averages $\langle\delta\phi_b(\tau)\rangle_{\phi^0}\left\langle\big(\delta(x_2(\tau) - x_2)\big)\right\rangle_{\phi^0}$ has similar behaviour and values but with opposite sign, which leads to significantly smaller values for the average $\langle\phi_b(\tau)(x_1(\tau) - x_1)\rangle_{\phi^0}$

The other average in the function $M^{\phi^0}(\tau, t)$ can be neglected.

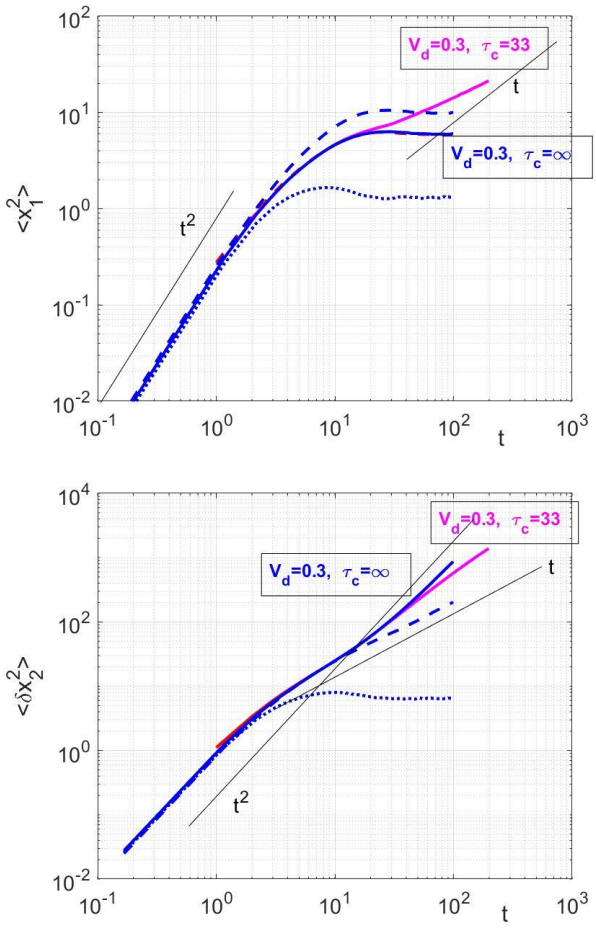

FIG. 8: Trajectory dispersion in the radial (left) and poloidal (right directions) in time dependent (magenta) and static (blue) potentials. Also shown are the dispersions of the trapped (pointed) and free (dashed) trajectories. The time variation of the potential (magenta) determines subdiffusive radial transport (not saturated) and superdiffusive poloidal transport (not ballistic).

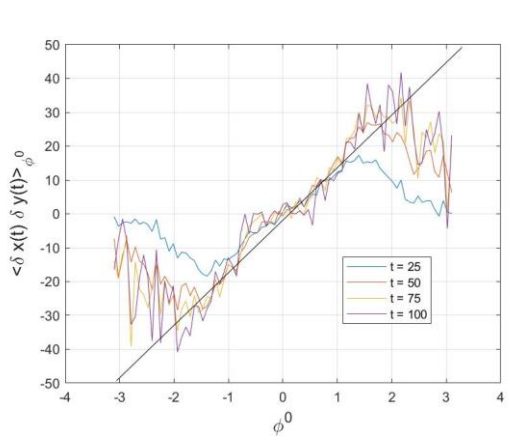

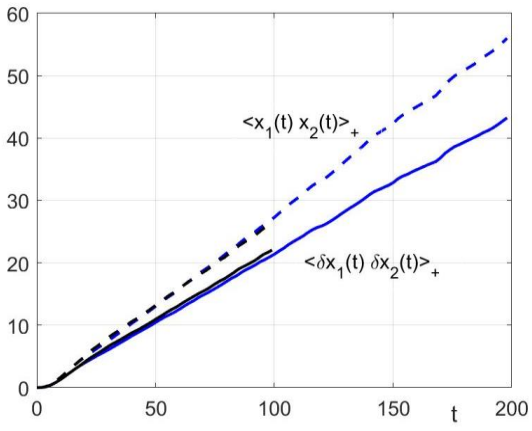

FIG. 9: The cross correlation of the displacements conditioned by ϕ^0 as function of ϕ^0 shows the approximate linearity in ϕ^0 (left). The time dependence of these correlation integrated aver positive ϕ^0 (right).

The dispersion relation of the test modes on turbulent plasma

Using the above statistical elements, the function $M^{\phi^0}(\tau,t)$ can be written as

$$\begin{aligned}
M^{\phi^0}(\tau,t) &= \exp\left[\phi^0 A + B + \text{sign}\,(\phi^0)C\right] \\
A &= \Phi\exp\left(-\tau/\tau_m\right)\left(1-\tfrac{\tau-t}{\tau_m}\right) + \tfrac{V_e}{c_s}g^{\zeta}\tfrac{\tau-t}{\tau_m} - k_1k_2\rho_s^2 g^{12} - ik_2\rho_s\tfrac{e\Phi}{T_e}g^{\phi 2} + ik_2\rho_s\tfrac{V_e}{c_s}g^{\zeta 2} \\
B &= \tfrac{e^2\Phi^2}{2T_e^2} - \tfrac{1}{2}k_i^2\tau_{fl}D_{ii}(\tau)(t-\tau) - ik_1\rho_s\tfrac{e\Phi}{T_e}g^{\phi 1} + ik_1\rho_s\tfrac{V_e}{c_s}g^{\zeta 1}\tfrac{\tau-t}{\tau_m} \\
C &= ik_1\tau_{fl}\langle v_1(\tau)\rangle_{sg}(t-\tau).
\end{aligned} \tag{10}$$

The integral over ϕ^0 has to be separately performed for positive and negative domains due to the term dependent on the sign of ϕ^0.

$$\begin{aligned}
\langle M(\tau,t)\rangle &= \int_{-\infty}^{\infty} d\phi^0 \langle M(\tau,t)\rangle_{\phi^0} P(\phi^0) \\
&= \frac{1}{\sqrt{2\pi}}\int_0^{\infty} d\phi^0 \exp\left[-\frac{(\phi^0)^2}{2} + \phi^0 A + B + C\right] + \int_{-\infty}^{0} d\phi^0 \exp\left[-\frac{(\phi^0)^2}{2} + \phi^0 A + B - C\right] \\
&= \exp\,(B+C)\left[\frac{1}{2} + \frac{A}{\sqrt{2\pi}}\right] + \exp\,(B-C)\left[\frac{1}{2} - \frac{A}{\sqrt{2\pi}}\right]
\end{aligned}$$

The time integral in the propagator is calculated by separating the time-dependent parts in the functions present in $\langle M(\tau,t)\rangle$

$$\begin{aligned}
A &= A_s + A_t(\tau - t) \\
A_s &= \Phi\exp\left(-\tau/\tau_m\right) - k_1k_2\rho_s^2 g^{12} - ik_2\rho_s\tfrac{e\Phi}{T_e}g^{\phi 2} + ik_2\rho_s\tfrac{V_e}{c_s}g^{\zeta 2} \\
A_t &= \Phi\exp\left(-\tau/\tau_m\right)\tfrac{1}{\tau_m} + \tfrac{V_e}{c_s}g^{\zeta}\tfrac{1}{\tau_m} \\
B &= B_s + B_t(\tau - t) \\
B_s &= \tfrac{e^2\Phi^2}{2T_e^2} - ik_1\rho_s\tfrac{e\Phi}{T_e}g^{\phi 1} \\
B_t &= \tfrac{1}{2}k_i^2\tau_{fl}D_{ii}(\tau) + ik_1\rho_s\tfrac{V_e}{c_s}g^{\zeta 1}\tfrac{1}{\tau_m} \\
C &= iC_t(\tau - t),\ C_t = -k_1\tau_{fl}\langle v_1(\tau)\rangle_{sg}
\end{aligned} \tag{11}$$

The integrals of the two terms of $\langle M(\tau,t)\rangle$ are

$$
\begin{aligned}
I_1 &= i\exp(B_s)\int_{-\infty}^{t} d\tau \left[\frac{1}{2}+\frac{A_s+A_t(\tau-t)}{\sqrt{2\pi}}\right]\exp\left[-(i\omega-B_t-iC_t)(\tau-t)\right] \\
&= \exp(B_s)\left[\frac{-\left(\frac{1}{2}+\frac{A_S}{\sqrt{2\pi}}\right)}{\omega-C_t+iB_t}+\frac{iA_t}{\sqrt{2\pi}(\omega-C_t+iB_t)^2}\right] \\
I_2 &= i\exp(B_s)\int_{-\infty}^{t} d\tau \left[\frac{1}{2}-\frac{A_s+A_t(\tau-t)}{\sqrt{2\pi}}\right]\exp\left[-(i\omega-B_t+iC_t)(\tau-t)\right] \\
&= \exp(B_s)\left[\frac{-\left(\frac{1}{2}-\frac{A_S}{\sqrt{2\pi}}\right)}{\omega+C_t+iB_t}-\frac{iA_t}{\sqrt{2\pi}(\omega+C_t+iB_t)^2}\right]
\end{aligned}
\tag{12}
$$

The propagator (3) is

$$
\bar{\Pi}_1^i = I_1 + I_2 \tag{13}
$$

The average in Eq. (4) can be calculated from

$$
\langle k_i v_{ib}(\tau) M(\tau)\rangle_{\phi^0} = \frac{d}{dc}\left\langle M(\tau)\exp\left(ck_i v_{ib}(\tau)\right)\right\rangle_{\phi^0}|_{c=0}
$$

The average in the rhs of this equation can be written as

$$
\begin{aligned}
&\frac{d}{dc}\left\langle M(\tau)\exp\left(ck_i v_{ib}(\tau)\right)\right\rangle_{\phi^0}|_{c=0} \\
&= \langle M(\tau,t)\rangle_{\phi^0}\frac{d}{dc}\exp\left[ck_i\langle v_{ib}(\tau)\rangle_{sg}\right] \\
&= \langle M(\tau,t)\rangle_{\phi^0}\left[k_i\langle v_{ib}(\tau)\rangle_{sg}+ik_ik_j\langle\delta v_{ib}(\tau)(x_i(\tau)-x_i)\rangle_{\phi^0}\right] \\
&= \langle M(\tau,t)\rangle_{\phi^0}\left[k_1\langle v_{1b}(\tau)\rangle_{sg}+ik_ik_jD_{ij}\right]
\end{aligned}
$$

because we have found that the correlations of the fluctuations of the velocity with the background potential and with the polarization drift are small and can be neglected. The average over the potential yields

$$
\begin{aligned}
&\int_{-\infty}^{\infty} d\phi^0\langle M(\tau,t)\rangle_{\phi^0}P(\phi^0)\left[k_1\langle v_{1b}(\tau)\rangle_{sg}+ik_ik_jD_{ij}^{\phi^0}\right] \\
&= k_1\langle v_{1b}(\tau)\rangle_{+}\exp(B+C)\left[\sqrt{\frac{\pi}{2}}+A\right]-k_1\langle v_{1b}(\tau)\rangle_{+}\exp(B-C)\left[\sqrt{\frac{\pi}{2}}-A\right]+ik_ik_jD_{ij}\langle M(\tau,t)\rangle
\end{aligned}
$$

The propagator (4) is

$$
\bar{\Pi}_2^i = k_1\langle v_{1b}(\tau)\rangle_{+}I_1 - k_1\langle v_{1b}(\tau)\rangle_{+}I_2 + ik_ik_jD_{ij}\bar{\Pi}_1^i \tag{14}
$$

The dispersion relation for test modes in turbulent plasma is

$$
\begin{aligned}
-\left(k_yV_{*e}-\omega\rho_s^2k_\perp^2\right)\bar{\Pi}_1^i-\bar{\Pi}_2^i &= 1+i\sqrt{\frac{\pi}{2}}\frac{\omega-k_yV_{*e}}{|k_z|v_{Te}} \\
-\left(k_yV_{*e}-\omega\rho_s^2k_\perp^2+ik_ik_jD_{ij}\right)(I_1+I_2)-k_1\langle v_{1b}(\tau)\rangle_{+}(I_1-I_2) &= 1+i\sqrt{\frac{\pi}{2}}\frac{\omega-k_yV_{*e}}{|k_z|v_{Te}}
\end{aligned}
\tag{15}
$$

Taking $A_t = 0$ because is small due to the factor $1/\tau_m$

$$I_1 + I_2 = \exp(B_s)\left[\frac{-\left(\frac{1}{2}+\frac{A_s}{\sqrt{2\pi}}\right)}{\omega - C_t + iB_t} + \frac{-\left(\frac{1}{2}-\frac{A_s}{\sqrt{2\pi}}\right)}{\omega + C_t + iB_t}\right]$$
$$= -\frac{\exp(B_s)}{(\omega - iB_t)^2 - C_t^2}\left[(\omega - iB_t) + \frac{A_s}{\sqrt{2\pi}}2C_t\right] \quad (16)$$
$$I_1 - I_2 = -\frac{\exp(B_s)}{(\omega - iB_t)^2 - C_t^2}\left[C_t + \frac{A_s}{\sqrt{2\pi}}2(\omega - iB_t)\right]$$

The dispersion relation (15) is rather complex. The effects of ion trajectory coherence strongly influence the propagator and determine a new term (the second in (15) that reflects the ordered radial displacements).

These results will be implemented in a code based on the iterated selfconsistent approach, which determines the evolution of turbulence from results of the dispersion relation and trajectory simulation [10]. The evolution of turbulence from a given initial spectrum with small amplitude is determined by a repeated sequence, which consists of:

1. solving the dispersion (15) for each mode;
2. determining the short time (of the order of τ_m) evolution of the spectrum from the growth rates and frequencies;
3. calculation of the trajectories in the new potential over the next interval τ_m, and of the statistical quantities in the dispersion equation.

Effects of the ion trajectory coherence in drift type turbulence

The main effects of coherence can be analyzed from the structure of the propagators and from the characteristics of the statistical quantities contained in the dispersion equation.

For small amplitude of the background potential ($(e\Phi)/T_e \ll \rho_s/L_n$), the time of flight is larger than the decorrelation time and trapping and coherence do not appear. The diffusion is normal with very small coefficients in both directions. The distribution of the displacements is Gaussian. The complex set of averages conditioned by ϕ^o that represent aspects of coherence does not exist. Then

$$A_s = 0, \qquad A_t = 0, \qquad B_s = 0, \qquad B_t = k_i^2 V_e \rho_s D_{ii}(\tau), \qquad C = 0,$$

which makes

$$I_1 = I_2 = \frac{1}{2(\omega + iB_t)}$$

and leads to the well-known results of turbulent attenuation of the large k modes

$$\gamma = \sqrt{\frac{\pi}{2}} \frac{\omega\left(k_y V_{*e} - \omega\right)}{|k_z| v_{Te}} - i k_i^2 V_e \rho_s D_{ii}$$

As turbulence amplitude increases due to the positive γ, the turbulence reaches the nonlinear regime ($(e\Phi)/T_e \sim \rho_s / L_n$), except for the cases of very small density gradients. The first effects are direct (increase of the terms that depend on Φ) and through correlations (namely the cross correlation of the displacements and correlation of the Lagrangian potential with the trajectories). The functions A_s and B_s begin to increase

$$A_s = \Phi \exp\left(-\frac{\tau}{\tau_m}\right) - k_1 k_2 \rho_s^2 g^{12} - i k_2 \rho_s \frac{e\Phi}{T_e} g^{\phi 2}, \qquad B_s = \frac{e^2 \Phi^2}{2 T_e^2} - i k_1 \rho_s \frac{e\Phi}{T_e} g^{\phi 1}.$$

First, the dominant effect is determined by B_s, which increases the frequencies. The effect of A_s only consists in the generation of a small difference between I_1 and I_2. The propagator $\bar{\Pi}_1^i$ is not dependent on A_s at this level of turbulence.

The main effect is produced at larger amplitudes, when the trapping is stronger and produces radial coherent displacements and memory effects that increase the coherence. It determine a weak time increase of $\langle x_1(\tau) - x_1(t) \rangle_{sg}$ and generates average perpendicular velocities. These effects appear in the dispersion relation (15) where the second term is not zero in these conditions and are also represented by the term C in the propagator. Both components are modified and the diference I_1-I_2 increases. This term is a new source of instability that adds to that determined by the density gradient when the amplitude of the background turbulence is large. It determines unstable modes completely different of the drift modes: with $k_y = 0$, $k_x \neq 0$ and very small frequencies, much smaller than the diamagnetic frequency, the zonal flow modes.

The evolution of the turbulence in this strongly nonlinear stage is rather complex. The memory effects make the frequencies and the growth rates dependent on time during intervals of the order τ_m. The radial coherence determines first the increase of the amplitude of the drift type turbulence despite the superdiffusive poloidal transport. The zonal flow modes are weakly affected by trajectory dispersion, which is subdiffusive along x_1, and they grow in this phase. This determines important modifications of the spectrum of the background potential, which acquires a new component in the domain that is stable for the drift modes ($k_y \cong 0$, k_x of the order $1/\langle x_1(\tau) - x_1(t) \rangle_{sg}$). The complexity of the evolution is very high in these conditions because the coherent motion influences the frequency and growth rate through all the statistical quantities that apper in Eq. (15). The background turbulence has complicated changes in its spectrum that have to be taken into account in the iterated selfconsistent approach. It is already rather clear that ϕ_b has not a smooth evolution, but is characterized by time fluctuations on the scale of τ_m.

Conclusions

The main findings of this work are:

- *A second source of instability, which develops as the amplitude of the turbulence increases*
  It is the second term in the dispersion relation (15) that is determined by the coherent motion in the radial direction. It is interesting to emphasize that this source acts only if $I_1 \neq I_2$, and that this difference exists only due to coherent aspects of turbulence.
- We have identified a new characteristic time in the statistics of trajectories and in the evolution of turbulence: the memory time τ_m.
- *The growth rates and the frequencies are intrinsically time-dependent*
  The characteristics of the turbulent potential are not smooth time functions, but they have oscillating evolution on time intervals of the order of τ_m. This is much longer than the correlation time $1/\gamma$ and corresponds to very small frequencies, much smaller than ω. Such evolution is in agreement with the results of the numerical simulations and of the experimental measurement.

We will examine in the next period the possibility of extracting characteristics of the turbulence from these oscillations.

[1] Krommes J. A., Phys. Reports 360, 1 (2002).

[2] Horton W, Rev. Modern Phys. 71, 735 (1999).

[3] Garbet X, Idomura Y, Villard L, Watanabe T H, Nuclear Fusion 50, 043002 (2010).

[4] Tynan G. R., Fujisawa A., McKee G., Plasma Phys. Control. Fusion 51, 113001 (2009).

[5] Diamond P. H., Hasegawa A., Kima K., Plasma Phys. Control. Fusion 53, 124001 (2011).

6] Terry PW, Rev. Mod. Phys. 72, 109 (2000)

[7] Diamond P. H., Itoh S.-I., Itoh K., Hahm T. S., Plasma Phys. Control. Fusion 47, R35-R161 (2005).

[8] Hasegawa A., Kima K., Phys. Fluids 21, 1 (1978).

[9] Hasegawa A., Wakatani M., Phys. Rev. Lett. 59, 1581 (1987).

[10] Vlad M, Spineanu F, Randon and quasi-coherent aspects in particle motion and their effects on transport and turbulence evolution, New Journal of Physics 19 (2017) 025014

[11] Vlad, Ion stochastic trapping and drift turbulence evolution, Physical Review E 87053105 (2013).

[12] T. Estrada, C. Hidalgo, T. Happel, and P. H. Diamond, Phys. Rev. Lett. 107, 245004 (2011).

[13] P. Xanthopoulos, A. Mischchenko, P. Helander, H. Sugama, and T.-H. Watanabe, Phys. Rev. Lett. 107, 245002 (2011).

[14] M. Xu et al., Phys. Rev. Lett. 108, 245001 (2012).

[15] L. Schmitz et al., Phys. Rev. Lett. 108, 155002 (2012).

[16] Zehua Guo, Liu Chen, and Fulvio Zonca, Phys. Rev. Lett. 103, 055002 (2009).

[17] P. Manz, M. Ramisch, and U. Stroth, Phys. Rev. Lett. 103, 165004 (2009).

[18] R. H. Kraichnan, Phys. Fluids 19, 22 (1970).

[19] Balescu R., Aspects of Anomalous Transport in Plasmas, Institute of Physics Publishing (IoP), Bristol and Philadelphia, 2005.

[20] Neuer M., Spatschek K. H., Phys. Rev. E 74, 036401 (2006).

[21] W. D. McComb, The Physics of Fluid Turbulence, Clarendon, Oxford, 1990.

[22] Vlad M., Spineanu F., Misguich J.H., Balescu R., Phys.Rev.E 58, 7359 (1998).

[23] Vlad M. and Spineanu F., Phys. Rev. E 70, 056304 (2004).

[24] Dupree T. H., Phys. Fluids 9, 1773 (1966).

[25] Dupree T. H., Phys. Fluids 15, 334 (1972).

[26] Vlad M., Spineanu F., Romanian Journal of Physics 56 Supplement, 23 (2011).

[27] Goldstone R. J. and Rutherford P. H., Introduction to Plasma Physics, Institute of Physics Publishing, Bristol and Philadelphia, 1995.

[28] Vlad M., Spineanu F., Benkadda S., Phys. Rev. Lett. 96, 085001 (2006).

[29] Vlad M., Spineanu F., Benkadda S., Plasma Phys. Control. Fusion 50, 065007 (2008).

Modelling of the transport-turbulence dependencies. Programming of Bayesian inference.

Introduction

Turbulence and turbulent transport remain, to the present day, some of the biggest challenges in the path towards achieving controlled thermo-nuclear fusion. Since every experimental device operates on high-temperature plasmas driven far from equilibrium, turbulence originating from small scale instabilities that extract energy from macroscopic gradients is a characteristic of fusion discharges almost universally. This is especially true for tokamak devices under the EUROfusion work-package WPTE, like ASDEX Upgrade, MAST-U, TCV, etc., where the team working on the current project is assigned various tasks.

Turbulent transport is one side of the problem and it raises many difficult questions such as the dependencies between plasma parameters and transport, how does turbulence drive transport, what

physical (microscopic) mechanisms are at play, and how can we accurately predict it. In this report, we attempt to provide some partial theoretical answers to some of these queries. We use a statistical model for turbulent transport that can describe the intricacies of gyro-center trajectories in environments resembling tokamaks. In practice, the model is implemented using a numerical Fortran code that has been applied to other problems of a similar nature [1-4]. Since our simulations are much faster than gyro-kinetic counterparts, they can be executed on modest CPU architectures. They produce a set of radial transport coefficients (diffusion and velocity). Particle distributions, magnetic configuration, plasma equilibrium, and statistical characteristics of turbulence constitute the input. As a result, the code permits the creation of injective relations between transport coefficients and tokamak (discharge) parameters. The former can be utilized to calculate the plasma's dynamical tendencies. Once such relations are found, even on a numerical level, they may provide information about the underlying physical mechanisms of the transport as well as strategies for mitigating its negative effects.

The purpose of the present report goes beyond the simulation and the understanding of underlying physics of turbulent transport. Our goal is to create analytical models, or at least approximations, for the relationships between parameters and transport. Should this be accomplished with adequate precision, it would serve as a valuable instrument for forecasting transport in various scenarios that may arise during plasma discharges or for investigating parametric spaces with unknown parameters. Generally speaking, turbulent features are used to depict the latter. In order to achieve this type of mathematical modelling through regression, we need to develop a numerical database of results. Any meta-parameters that will arise in the analytical expressions of the regression models will be evaluated using such a database. Moreover, the latter will serve as learning and testing grounds for machine learning tools in a future phase of the project when different instruments such as feed-forward, deep-learning, and Bayesian neural networks will be developed. The latter may avoid the requirement for an approximate regression model and enable a quick and precise way to forecast turbulent transport.

Theory

We describe here, in short, the transport model, the statistical approach, and the numerical details of the code. The latter is already fully developed from the previous stage of the present project; thus, there have been no relevant new additions to it.

We consider a tokamak device that generates a macroscopic, external, magnetic field configuration $\boldsymbol{B}$. This field is space-dependent and its field-lines are tangent to the unit vector $\boldsymbol{b} = \boldsymbol{B}/|\boldsymbol{B}|$. In order to simplify our numerical scheme, we assume a concentrical, axisymmetric configuration in which:

$$\boldsymbol{B} = \frac{B_0 R_0}{R}(\vec{e}_\varphi + b_\theta(r)\vec{e}_\theta)$$

The standard definition of toroidal coordinates r, θ, φ has been used, as well as R_0 the large radius of the tokamak, B_0 the major axis magnetic field value and $R = R_0 + r\ cos\theta$. The radial term $b_\theta(r)$ is related to the poloidal magnetic component $\boldsymbol{B} \cdot \vec{e}_\theta$ and can be analytically captured by the poloidally averaged

safety factor $q(r) \approx 1 + 3\ (r/a)\text{^}2$ through the relation $b_\theta(r) = r/q(r)\sqrt{R_0^2 - r^2}$. In these definitions, a is the minor radius.

The plasma equilibrium is described, locally, by the density $n(r)$, temperature $T(r)$ and pressure $P(r)$. In particular, the temperature gradients $L_{T_{i,e}} = \nabla ln T_{i,e}$ have an important role in the determination of the diamagnetic velocities $\boldsymbol{V_i^\star} = -\hat{\boldsymbol{e}}_\perp v_{th}\rho_i/L_{T_i}$ $\boldsymbol{V_e^\star} = +\hat{\boldsymbol{e}}_\perp v_{th}\rho_i/L_{T_e}$ that induce the turbulence drift, either for ITG or TEM. Also, locally, we can compute the Larmor radius $\rho_i = m_i v_{th}/|e|B_0$, the thermal velocity $v_{th} = \sqrt{T_i/m_i}$. Supplementary, a toroidal plasma rotation $\boldsymbol{u}$ can be assumed.

A charged particle of mass and charge (m, q) is described by its gyro-center trajectory $\{\boldsymbol{X}(t), v_\parallel(t), \mu\}$ and obeys the following equations of motion:

$$\begin{cases} \dfrac{d\boldsymbol{X}(t)}{dt} = \boldsymbol{u} + v_\parallel \dfrac{\boldsymbol{B}^\star}{B_\parallel^\star} + \dfrac{\boldsymbol{E}^\star \times \boldsymbol{b}}{B_\parallel^\star} + \boldsymbol{\eta} \\ \dfrac{dv_\parallel}{dt} = \dfrac{q}{m}\dfrac{\boldsymbol{E}^\star \boldsymbol{B}^\star}{B_\parallel^\star} \\ \boldsymbol{B}^\star = \nabla \times \boldsymbol{A}^\star \quad ;; \quad \boldsymbol{E}^\star = -\boldsymbol{\nabla}\phi^\star - \partial_t \boldsymbol{A}^\star \\ \boldsymbol{A}^\star = \boldsymbol{A} + \dfrac{m}{q}(v_\parallel \boldsymbol{b} + \boldsymbol{u} + \boldsymbol{v}_E) \\ \phi^\star = \phi + \dfrac{\mu}{q}B - \dfrac{m\boldsymbol{u^2}}{2q} \end{cases}$$

In these expressions, $\boldsymbol{v_E} = \boldsymbol{b} \times \boldsymbol{\nabla}\phi/\mathrm{B}$ isthe standard $\boldsymbol{E} \times \boldsymbol{B}$ drift, $\boldsymbol{\eta}$ is the collisional velocity, $B_\parallel^\star = \boldsymbol{B}^\star \cdot \boldsymbol{b}$ while $v_\parallel$ and μ are the parallel velocity and the magnetic moment in the local frame which moves with the plasma flow $\boldsymbol{u}$.

Finally, the turbulence is considered a mix between Ion Temperature Gradient and Trapped Electron Mode (ITG, TEM). This means that the turbulent potential $\phi(\boldsymbol{x}, t)$ is a superposition of two random fields. The distribution is assumed normal (Gaussian) and homogeneous. Such statistical properties are in line with experimental and gyrokinetic results. The wave-number spectrum is drift-like and modelled analytically as:

$$S_s(\boldsymbol{k}) \sim e^{-\frac{k_r^2\lambda_r^2}{2} - \frac{k_\parallel^2\lambda_\parallel^2}{2}} k_\perp \left(e^{-\frac{(k_\perp - k_0^s)^2\lambda_\perp^2}{2}} - e^{-\frac{(k_\perp + k_0^s)^2\lambda_\perp^2}{2}} \right)$$

The wave frequency modes are approximated as non-interacting and obey a linear dispersion relation:

$$\omega_s(\boldsymbol{k}) = \boldsymbol{k} \cdot \boldsymbol{V_i^\star} \frac{T_e}{T_i} \frac{1}{1 + (T_i/T_e)^2 \rho_i^2 (k_r^2 + k_\perp^2)}$$

The Fourier representation of such turbulent fields in a single random realization is:

$$\phi_{\boldsymbol{k}}(t) = \Phi \left(\sqrt{A_i S_i(\boldsymbol{k})}\xi_i(\boldsymbol{k}) e^{-i\,\omega_i(\boldsymbol{k})t} + \sqrt{A_e S_e(\boldsymbol{k})}\xi_e(\boldsymbol{k}) e^{-i\,\omega_e(\boldsymbol{k})t} \right)$$

The A_i, A_e are fractions of each instability such that $A_i + A_e = 1$, Φ is interpreted as the overall turbulence amplitude while $S_i(\boldsymbol{k}), S_e(\boldsymbol{k})$ are spectra associated with ITG and TEM turbulence. The fields $\xi_i(\boldsymbol{k}), \xi_e(\boldsymbol{k})$ are independent white noises $\langle \xi_s(\boldsymbol{k}) \rangle = 0$ and $\langle \xi_s(\boldsymbol{k}) \xi_{s'}(\boldsymbol{q}) \rangle = \delta_{s,s'}\delta(\boldsymbol{k} + \boldsymbol{q})$.

The main idea of the statistical approach is as it follows. One generates a statistical ensemble of random fields $\{\phi(\boldsymbol{x},t)\}$ with the prescribed statistical properties (distribution, spectrum). For each such realization and each possible kinetic property of a particle (initial parallel velocity $v_{\parallel}$, magnetic moment μ and initial position $\boldsymbol{X}(t=0)$) a trajectory is computed with the aid of the equations of motion written above. The statistical averages of these trajectories and their spreading across the whole ensemble are directly linked with the transport coefficients: velocity V and diffusion D. The latter are the quantities of interest.

From numerical perspectives, we solve the equations using a 4th order Runge-Kutta method for a numerical statistical ensemble of $N_p = 10^5$ particles/field realizations. Each field-realization is build with the aid of a discrete Fourier decomposition in $N_c = 500$ partial waves:

$$\phi(\boldsymbol{x},t) = \sqrt{\frac{2}{N_c}}\left(\sum_{j=1}^{N_c^i}\sin\left(\boldsymbol{k_j^i}\boldsymbol{x} - \omega_i(\boldsymbol{k_j^i})t + \alpha_j^i\right) + \sum_{j=1}^{N_e^i}\sin\left(\boldsymbol{k_j^i}\boldsymbol{x} - \omega_i(\boldsymbol{k_j^i})t + \alpha_j^i\right)\right)$$

Here, α_j^e, α_j^i are independent uniformly distributed phases $\in (0,2\pi)$, the vectors $\boldsymbol{k_j^e}, \boldsymbol{k_j^i}$ are random vectors distributed accordingly with the PDFs $S_e(\boldsymbol{k_j^e}), S_i(\boldsymbol{k_j^i})$. The number of partial waves are chosen $N_c^i = N_c A_i, N_c^e = N_c A_e$ such that the fractions of ITG, TEM are well reproduced $N_c^i + N_c^e = N_c$.

Numerical simulations and database

The goal of this work is to find, understand and model mathematically the relationship between turbulent transport coefficients and tokamak plasma parameters. Since the problem is highly-nonlinear, this can be achieved only through numerical means. We aim first at getting a large set of data that will become a database for the injective relation between parameters P and transport coefficients V, D, thus $P \to D, V$.

We choose the case of the ASDEX Upgrade tokamak as being medium-sized and representing a "middle-point" in the parametric space of existing tokamak devices. In the Table 1 shown below are described the fundamental parameters of our model with their interpretation. The "reference value" corresponds to AUG standard discharges. The interval of variation refers to the parametric space where we intend to investigate their impact on the transport, the central query of this work.

Parameter	Interpretation	Reference value	Interval of variation
T_i	Ion temperature	$1\ keV$	$[0-2]keV$
T_e	Electron temperature	$1\ keV$	$[0-2]keV$
B_0	Magnetic field value near axis	$2.5\ T$	$[0-4]T$
R_0	Large radius	$1.65\ m$	$[0.8-2.5]m$
a	Small radius	$0.65\ m$	$[0.3-0.8]m$

n_0	Plasma density	$10^{19}m^{-3}$	$[1-6]10^{19}m^{-3}$
Ω_t	Toroidal plasma rotation	$10^4 Hz$	$10^4[0-5]Hz$
T	Species temperature	T_i	$[0-2]T_i$
r_0	Initial position	$a/2$	$[0.1-1]a$
L_{T_i}	Ion temperature gradient	$R_0/5$	$R_0/[1-10]$
λ_x	Radial correlation length	$6\rho_i$	$[2-10]\rho_i$
λ_y	Poloidal correlation length	$6\rho_i$	$[2-10]\rho_i$
λ_z	Toroidal correlation length	a	$[0.3-2]a$
k_0	Dominant wave number	$0.1/\rho_i$	$[0-0.5]/\rho_i$
Φ	Turbulence amplitude	3%	$[0-7]\%$
L_{T_e}	Electron temp. Gradient	$R_0/5$	$R_0/[1-10]$

Table 1: The main parameters of the model, their reference value coresponing to AUG like discharges and the interval of variation of each parameter.

Results

Here, we present the numerical radial diffusion dependency on each parameter, as determined by numerical simulations. Additionally, we include a regression approximation for each dependency. All these results are shown in the Figs. [1-5] bellow. The red dots are real numerical values of the diffusion. The blue lines (and the blue dots) represent the proposed regression model. The latter is motivated by our need to balance analytical simplicity and the ability to reproduce the "exact" numerical values.

Note that many real dependencies (red) are plagued with some level of randomness (oscillations). These are of numerical nature and are quite difficult to remove. The only cure is to increase the number of test-particles $\mathrm{N_p}$ but the errors decrease only as $\mathrm{N_p^{1/2}}$ which means that a large numerical effort is required. In order to lower the fluctuations by a factor of 3, the computing time must be increased almost ten fold. Since the regression approach itself is an approximation, we have considered that a superior level of accuracy would have required an unacceptable level of CPU resources and was not necessary at this stage.

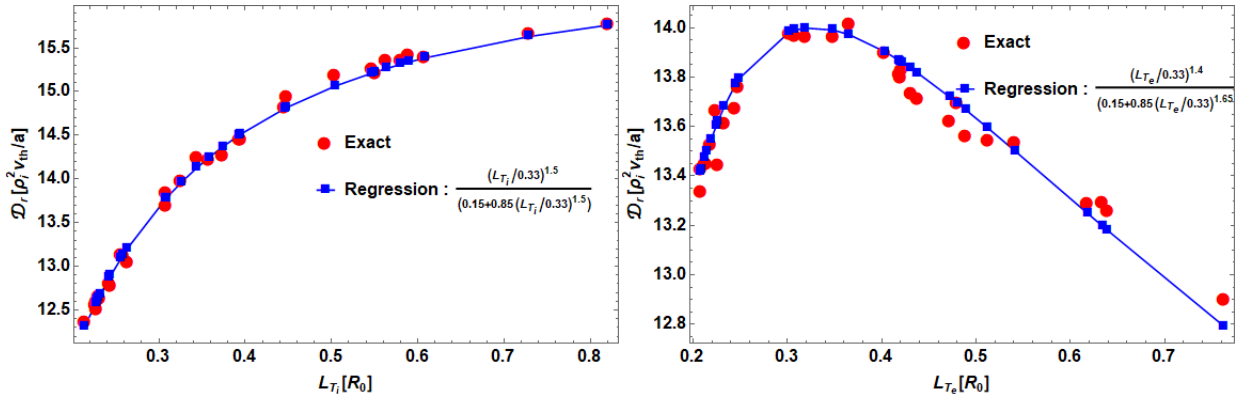

Fig. 1: The dependency between radial diffusion D_r and ion/electron temperature gradient $L_{T_{i/e}}$ obtained with nonlinear numerical simulations (red) and fitted with a regression model (blue).

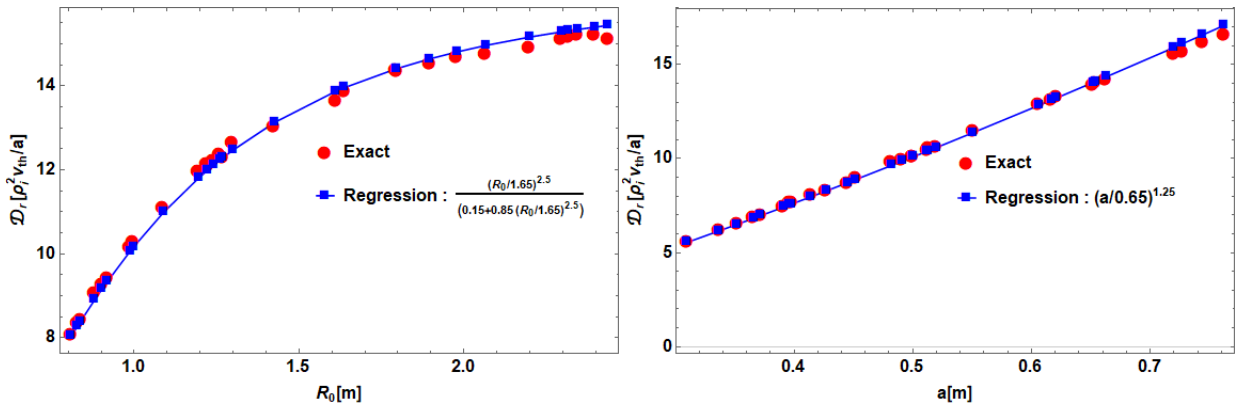

Fig. 2: The dependency between radial diffusion D_r and major/minor radius of the tokamak R_0/a obtained with nonlinear numerical simulations (red) and fitted with a regression model (blue).

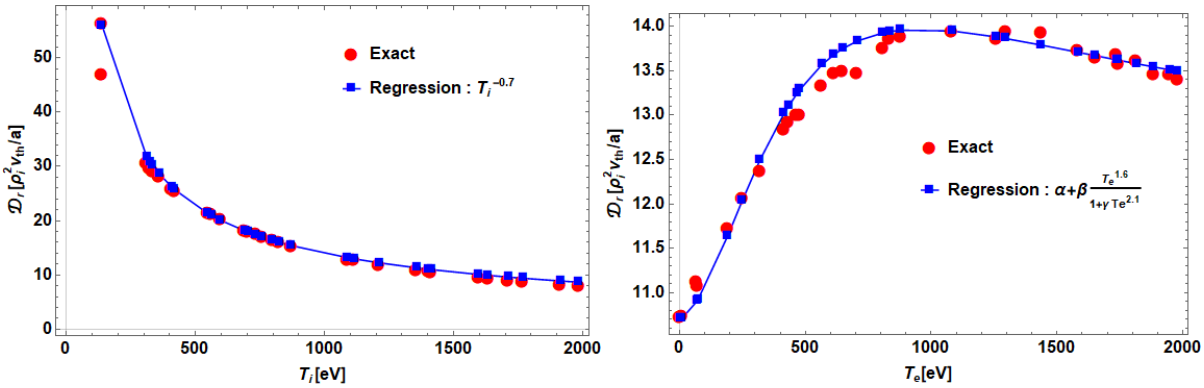

Fig. 3: The dependency between radial diffusion D_r and ion/electron temperature T_i/T_e obtained with nonlinear numerical simulations (red) and fitted with a regression model (blue).

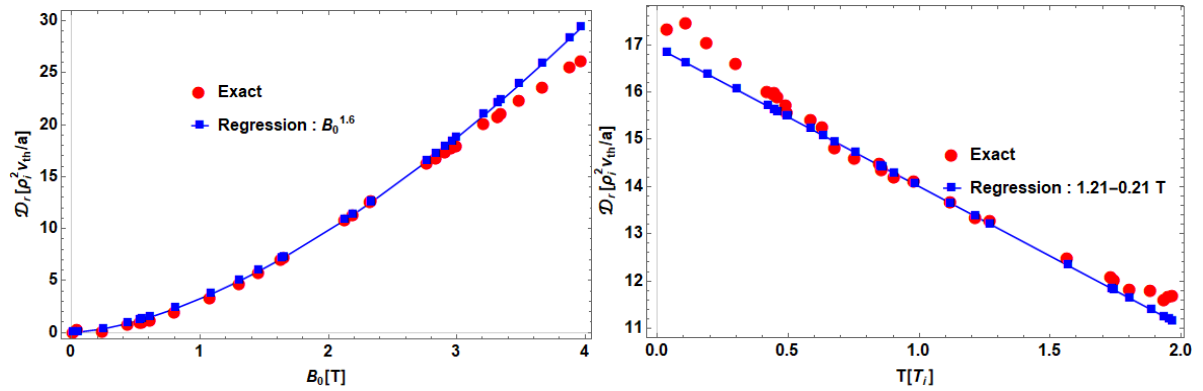

Fig. 4: The dependency between radial diffusion D_r and magnetic field intensity B_0 and species temperature T obtained with nonlinear numerical simulations (red) and fitted with a regression model (blue).

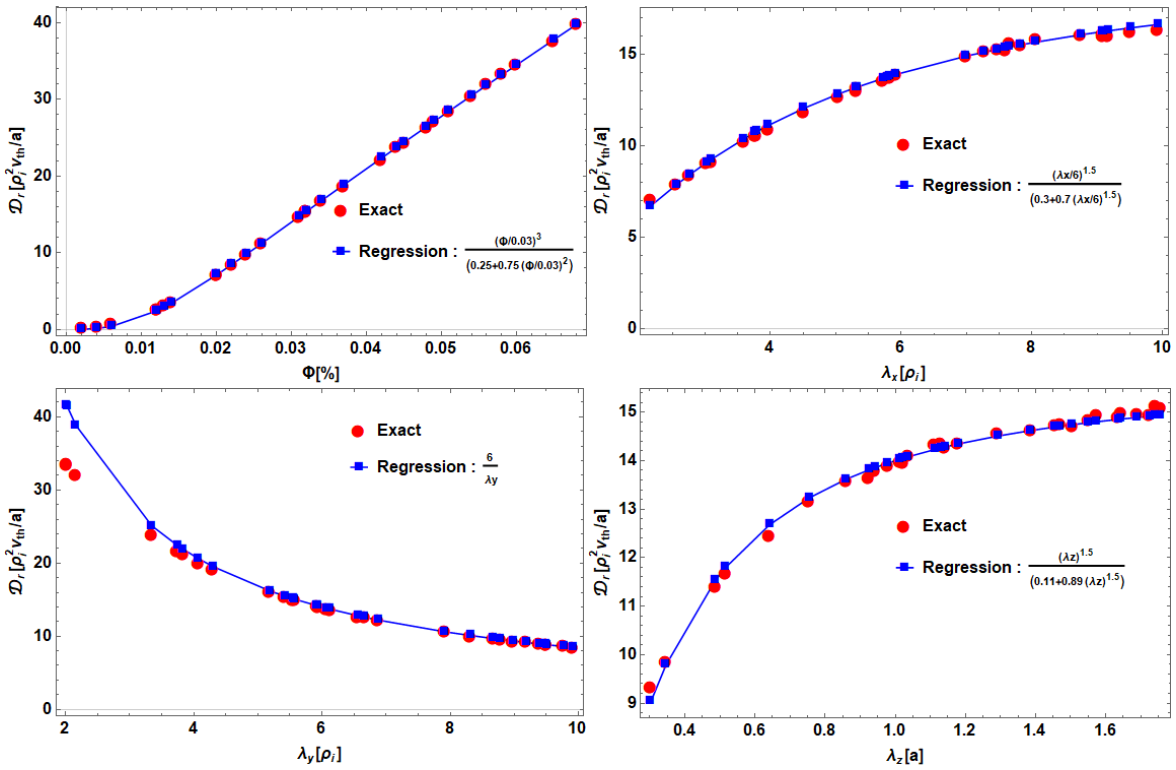

Fig. 5: The dependency between radial diffusion D_r and turbulence spectral properties: amplitude Φ and correlation lengths $\lambda_x, \lambda_y, \lambda_z$ obtained with nonlinear numerical simulations (red) and fitted with a regression models (blue).

Once the individual dependencies around the baseline scenario have been obtained and appropriate regression formulas have been found, it is time to determine to what degree this mathematical modelling can reproduce data in scenarios that depart more from the baseline. A technical difficulty appears: the information encoded in the regressions shown in Figs. [1-5] is valid only when all parameters are constant but one. How can we expand this information to the entire many-dimensional domain? We choose the simplest strategy of all: we consider that the multi-varied dependency of diffusion D_r on parameters $P = \{T_i, T_e, B_0, a, \lambda_x, \lambda_y, \lambda_z, \Phi, R_0, L_{T_i}, L_{T_e}\}$ can be factorized on single-varied dependencies. The result is the formula described bellow:

$$D_r = D_r(ref)\frac{6}{\lambda_y}\left(\frac{T_i}{10^3}\right)^{-0.7}\left(\frac{B_0}{2.5}\right)^{1.6}\left(\frac{a}{0.65}\right)^{1.25}\frac{(\lambda x/6)^{1.5}}{0.3+0.7(\lambda x/6)^{1.5}}\frac{10.7/14+1.05\left(\frac{T_e}{10^3}\right)^{1.6}}{1+3.5\left(\frac{T_e}{10^3}\right)^{2.1}}\frac{\left(\frac{\Phi}{0.03}\right)^2}{0.25+0.75\left(\frac{\Phi}{0.03}\right)^2}(1.21 - 0.21T)\frac{\left(\frac{R_0}{1.65}\right)^{2.5}}{0.15+0.85\left(\frac{R_0}{1.65}\right)^{2.5}}\frac{\left(\frac{L_{T_i}}{0.33}\right)^{1.5}}{0.15+0.85\left(\frac{L_{T_i}}{0.33}\right)^{1.5}}\frac{\left(\frac{L_{T_e}}{0.33}\right)^{1.4}}{0.15+0.85\left(\frac{L_{T_e}}{0.33}\right)^{1.65}}\frac{\lambda_z^{1.5}}{0.11+0.89\lambda_z^{1.5}}$$

To test weather this global model bears any meaning in realistic situation, we have performed a set of $N_d = 200$ numerical simulations using randomly generated parameters that fall within the ranges of variations described in Table 1. For each such set, the exact diffusion is evaluated and compared with the one predicted by the global formula shown above. The results are plotted in Fig [6] as regression vs exact values. We observe an appropriate degree of agreement, aside from several outliers. While the latter might seem to imply an important failure of our model, we note that they happen at small values of diffusion which are, by themselves, irrelevant. Moreover, when diffusion is small, the numerical results of the code are plagued with a larger degree of relative error which makes the data uncertain. We conclude at this end that the minimal mathematical model developed is relatively precise on large datasets, but supplementary improvements should be developed in the future stage of the project.

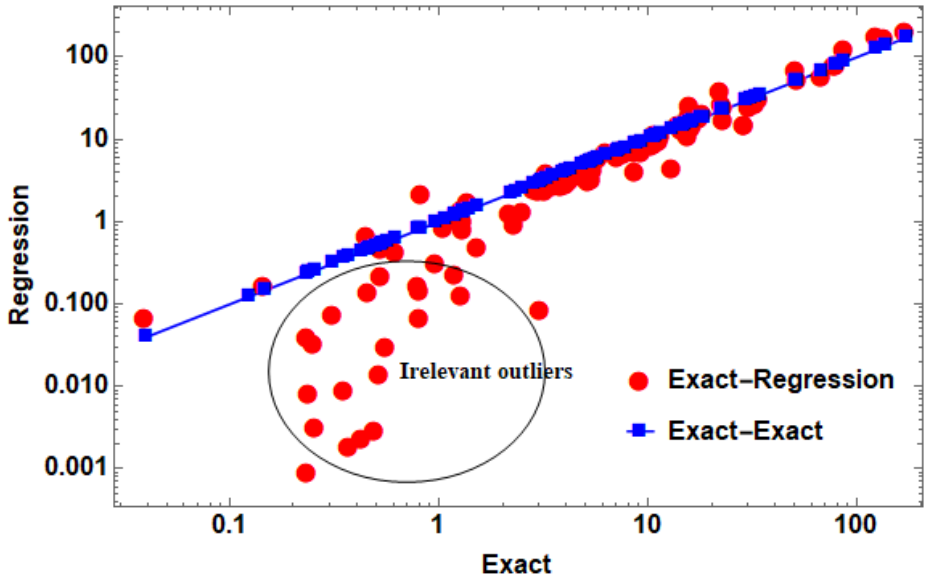

Fig. 6: Radial diffusion coefficients obtained with the regression model vs exact radial diffusions obtained with nonlinear numerical simulations. Note that the outliers are irrelevant since they correspond to small values of the diffusion coefficients which are not only uninteresting, but are also plagued with large relative errors.

Preparing the grounds for machine learning/Bayesian approaches

In the next phase of the present project, the database will grow to be truly "extensive", with the performance of approximately 10^5 simulations. This will enable the collection of enough data to support the creation of a machine-learning techniques as tools for transport forecasting. In this regard, we expect that Feed-Forward and Bayesian neural network will play an important role.

For that, we have acquired a basic understanding of the intricate mathematics underlying the concept of neural networks. Additionally, self-made feed-forward numerical codes have been created. Mathematica Wolfram is the language used to write such simple examples. Similar to preconstructed neural networks that are already available in Mathematica/Python, they have demonstrated good learning properties after

being trained on synthetic data. A sample of the self-made neural network and its training phase via the ADAM algorithm is displayed in Fig. [7].

```
(*ADAM*)

For[i = 1, i ≤ m + 1, i++, mW_i = 0.0 RandomReal[{0, 1}, {P[[i]], P[[i - 1 + δ_{i,1}]]}];
  mB_i = 0.0 RandomReal[{0, 1}, P[[i]]];
  vW_i = 0.0 RandomReal[{0, 1}, {P[[i]], P[[i - 1 + δ_{i,1}]]}];
  vB_i = 0.0 RandomReal[{0, 1}, P[[i]];];

α = 0.001; β1 = 0.90; β2 = 0.94; μ = 0.0; ϵ = 10^-8; maxepoch = 100000;
Clear[epoch]; Monitor[For[epoch = 1, epoch ≤ maxepoch, epoch++,
  For[j = 2, j ≤ m + 1, j++, int = B_j + W_j.Z_{j-1}; Z_j = f_j[int]; Zp_j = fp_j[int];];
  error_epoch = 1 / n1 Total[(Y - Z_{m+1})^2 // Flatten]; (*good*)
  For[j = 2, j ≤ m + 1, j++, int = B_j + W_j.Zval_{j-1}; Zval_j = f_j[int];];
  err2_epoch = 1 / (n - n1) Total[(Yval - Zval_{m+1})^2 // Flatten]; (*good*)
  D1_{m+1} = (Z_{m+1} - Y) Zp_{m+1};
  For[j = m, j ≥ 1, j--, D1_j = (Transpose[W_{j+1}].D1_{j+1}) Zp_j;];
  For[j = 2, j ≤ m + 1, j++,
   gB = Total[D1_j, {2}]; gW = (D1_j.Transpose[Z_{j-1}]);

   mB_j = β1 mB_j + (1 - β1) gB;
   mW_j = β1 mW_j + (1 - β1) gW;

   vB_j = β2 vB_j + (1 - β2) gB^2;
   vW_j = β2 vW_j + (1 - β2) gW^2;

   mB_j = mB_j / (1 - β1^epoch);
   mW_j = mW_j / (1 - β1^epoch);

   vB_j = vB_j / (1 - β2^epoch);
   vW_j = vW_j / (1 - β2^epoch);

   B_j = B_j - α mB_j / (ϵ + Sqrt[vB_j]);
   W_j = W_j - α mW_j / (ϵ + Sqrt[vW_j]);];
  keep_epoch = Z_{m+1};], {epoch, Sqrt[error_{epoch-1}] / norm}]
```

Fig. 7: A snapshot of the self-made code for the implementation of a general feed-forward neural networks optimized with the ADAM algorithm.

References

[1] Palade, D.I., Vlad, M. Stat Comput 31, 60 (2021).
[2] Madalina Vlad et al 2021 Plasma Phys. Control. Fusion 63 035007
[3] Dragos Iustin Palade et al 2021 Nucl. Fusion 61 116031
[4] D.I. Palade 2023 Nucl. Fusion 63 046007
[5] Alain J. Brizard; Phys. Plasmas 1 September 2013; 20 (9): 092309
[6] G M Staebler et al 2021 Plasma Phys. Control. Fusion 63 015013

Acknowledgement

This work has been carried out within the framework of the EUROfusion Consortium, funded by the European Union via the Euratom Research and Training Programme (Grant Agreement No 101052200 — EUROfusion). Views and opinions expressed are however those of the author(s) only and do not necessarily reflect those of the European Union or the European Commission. Neither the European Union nor the European Commission can be held responsible for them.

The research work presented here has been developed together people from Consortio RFX, Padua, Italy (A. Murari) and University of Rome "Tor Vergata" (Emmanuele Peluso, Michela Gelfusa, L. Spolladore) and Institute of Applied Physics, TU Wien, Fusion@ÖAW, Vienna, Austria (G. Harrer).

Conclusion

One of the objectives of the present project is to simulate, understand, and mathematically model the relationship between turbulent transport and plasma parameters. This was accomplished by means of extensive numerical simulations using a numerical Fotran code, that was created to implement a statistical transport model by representing turbulence as a statistical ensemble of random fields with predetermined statistical properties. AUG-like discharges were selected as the reference case. Around this central value, all the parameters are freely adjusted. We can obtain individual transport dependencies with the parameters by performing individual variations. These relations were mathematically modeled through an approach akin to regression. We also incorporate the analytical expression for regression into a single, all-inclusive formula. We demonstrate that the latter is not limited in its relevance, even though it is more precise unidimensionally, in the multi-dimensional parametric space. It can forecast random configurations of any tokamak devices within certain error bounds. Future developments (improvements) of the regression models are expected.

The statistical method of test-particles was also used in conjunction with an analytical analysis for the effect of hidden coherent components of motion on growth rates of drift-type turbulence. During this analysis it was found that: there is *a second source of instability, which develops as the amplitude of the turbulence increases,* the second term in the dispersion relation (15) that is determined by the coherent motion in the radial direction. We have identified a new characteristic time in the statistics of trajectories and in the evolution of turbulence: the memory time τ_m. *The growth rates and the frequencies are intrinsically time-dependent.* The characteristics of the turbulent potential are not smooth time functions, but they have oscillating evolution on time intervals of the order of τ_m. This is much longer than the correlation time $1/\gamma$ and corresponds to very small frequencies, much smaller than ω. Such evolution is in agreement with the results of the numerical simulations and of the experimental measurement.

a